NASA Technical Memorandum 107117

# Numerical Simulation of Flow in a Whirling Annular Seal and Comparison With Experiments

M.M. Athavale
*CFD Research Corporation*
*Huntsville, Alabama*

R.C. Hendricks and B.M. Steinetz
*Lewis Research Center*
*Cleveland, Ohio*

Prepared for the
Sixth International Symposium on Transport Phenomena and
Dynamics of Rotating Machinery
cosponsored by the Pacific Center of Thermal Fluids Engineering
and the U.S. Turbo and Power Machinery Research Center
Honolulu, Hawaii, February 25–29, 1996


National Aeronautics and
Space Administration

# Numerical Simulation of Flow in a Whirling Annular Seal and Comparison With Experiments

**M.M. Athavale**
*CFD Research Corporation, Huntsville, Alabama U.S.A. 35805*

**R.C. Hendricks and B.M. Steinetz**
*NASA Lewis Research Center, Cleveland, Ohio U.S.A. 44135*

## ABSTRACT

The turbulent flow field inside a whirling annular seal was simulated by using SCISEAL, a three-dimensional computational fluid dynamics code. The rotor center described a circular synchronous whirl. A rotating frame transformation was used to make the problem quasi-steady. The flow field at an axial Reynolds number of 24 000 and a Taylor number of 6600 was simulated. The standard $k$-$\varepsilon$ model with wall functions and the low-Reynolds-number model were used to treat turbulence. An experimentally measured velocity field was used at the inlet boundary. Numerical predictions of the velocities and the stator wall pressures compared well with experimental data. Both turbulence models yielded nearly the same results. The capability of the SCISEAL code to analyze this complex flow field was demonstrated; the isotropic turbulence models performed adequately on this nonisotropic turbulence flow.

Keywords: Seal; Rotordynamic; CFD; Turbulence; Modeling; Bearings; Tribology

## NOMENCLATURE

| | |
|---|---|
| $C$ | nominal clearance between stator and rotor, m |
| $D$ | rotor diameter, m |
| $e$ | rotor eccentricity, m |
| $k$ | turbulence production |
| $L$ | seal length, m |
| $P$ | static pressure, Pa |
| $P^*$ | nondimensional pressure, $PL/(C\ \Delta P)$ |
| $\Delta P$ | pressure drop across seal, (80.8 kPa for present case) |
| $R$ | rotor radius, m |
| Re | Reynolds number, $2\ C\rho U_m/\mu$ |
| $\vec{r}, \vec{R}$ | position vectors, m |
| Ta | Taylor number, $[\rho w_{sh} C/\mu][2C/D]^{1/2}$ |
| $U_m$ | mean axial velocity, m/s |
| $u, v, w$ | Cartesian velocity components, in $x$, $y$, and $z$ directions, m/s |
| $u_\theta, u_r, u_x$ | cylindrical velocity components in tangential, radial, and axial directions, m/s |
| $\vec{v}$ | velocity vector, m/s |
| $u_\theta^*, u_r^*, u_x^*$ | normalized velocity components |
| $w_{sh}$ | rotor surface tangential velocity, m/s |
| $X, Y, Z$ | Cartesian reference directions |
| $\varepsilon$ | orbit radius, m |
| $\mu$ | dynamic viscosity, Pa-s |
| $\rho$ | fluid density, kg/m$^3$ |
| $\Omega$ | rotor whirl angular velocity, rad/s |
| $\omega$ | rotor spin angular velocity rad/s |

**Subscripts:**

| | |
|---|---|
| $a$ | absolute |
| $r$ | rotor; relative |
| $s$ | stator |

## 1. INTRODUCTION

Turbomachinery seals are usually noncontacting and allow a leakage flow. Since the clearances are small, variations in the rotor position during operation can alter the fluid flow and the fluid reaction forces. The change in reaction forces can destabilize the rotor (e.g., a labyrinth seal) or provide stability (e.g., a damper seal). Evaluation of seal rotordynamic forces has long been a topic of interest. Black's [1] treatment is one of the early efforts. Subsequent methods include the bulk flow models developed by Childs [2]. Later refinements include two-dimensional models [3] where averaged film properties are used. Recent advances in computational fluid dynamics (CFD) methods have prompted the development of three-dimensional Navier-Stokes (N–S) codes for seal flow and rotordynamic analyses. Tam et al. [4] conducted a detailed study of the flow in seals to calculate the rotordynamic coefficients and to show the complexities of flows in whirling seals. A perturbation method based on finite-difference techniques was developed by Dietzen and Nordmann [5]. A finite-element perturbation model based on Navier-Stokes solutions was developed by Baskharone and Hensel [6,7] for seal rotordynamics. SCISEAL, a three-dimensional CFD code based on N–S equations and offering capabilities such as rotordynamics and different turbulence models, has been developed by Athavale et al. [8–10].

The current state-of-the-art codes rely on a variety of turbulence models to treat the turbulent flow fields that exist in turbomachinery seals. These models assume isotropic turbulence, and it is necessary to assess the accuracy of the results produced. Detailed flow-field measurements in seals for code validation are very few. Some studies deal with integrated quantities, such as rotor loads and rotordynamics (e.g., [11] and [12]). Laser Dopler anemometer measurements of flow and turbulence in annular and labyrinth seals were reported by Morrison et al. [13,14] for centered seals. The SCISEAL code was used to simulate these flows, and good correlation between the experiments and the numerical results was obtained [8].

Recently, Thames [15], Morrison et al. [16,17], and Winslow [18] have reported velocity, pressure, and shear stress measurements in a synchronous whirling annular seal. This problem is important in rotor stability because the two most unstable flow-related modes in an annular seal are the rotor whirl at subsynchronous and synchronous whirl speeds. Such experimental data can be important in validating CFD codes. The experiments were done on a seal with a large clearance-to-radius $C/R$ ratio (0.015); the practical values are near 0.0015. The size of the laser probe volume dictated the clearance used in the seal. For practical $C/R$ ratios, rigs with larger radius seals should be constructed and used.

The present study was done with multiple motives. One was to assess the accuracy of the physical models used in the code for rotating frames. Another was to check the performance of the two most commonly used turbulence models: the standard $k$-$\varepsilon$ model with wall functions, and the low-Re model (both assume isotropic turbulence) in a rotating reference frame and on an nonisotropic turbulence problem. The rotor whirl solution is also used to calculate seal rotordynamic coefficients, and thus the accuracy of these results is directly related to seal dynamics.

## 2. NUMERICAL METHODOLOGY

The computations were performed by using SCISEAL, an advanced three-dimensional CFD code developed under NASA sponsorship for the flow and force analysis of a variety of turbomachinery seals [8–10]. The code uses a pressure-based solution methodology to integrate the Navier-Stokes equations in the generalized body-fitted-coordinate (BFC) system. A finite-volume method is used to discretize the flow domain, and a collocated variable arrangement is used where all the velocity and scalar variables are stored at the center of each computational cell. Cartesian velocity components

are used as the primary velocity variables. The N–S equations are discretized and solved sequentially. A variation of the SIMPLEC method is used to provide the pressure-velocity coupling. High-order spatial and temporal discretization methods are available. A variety of turbulence models, including the standard and low-Re $k$-$\varepsilon$ models and a two-layer $k$-$\varepsilon$ model, are available in SCISEAL. The whirling seal problem was treated in this study by using the standard $k$-$\varepsilon$ model with wall functions. The experimental data include measurements of Reynolds stresses as well and could be used to validate models that predict nonisotropic turbulence.

## 3. WHIRLING SEAL GRID TRANSFORMATION

The whirling rotor generates a deforming or moving grid problem. A moving grid algorithm available in SCISEAL could be used, but such a time-dependent solution is expensive. When the whirl orbit is circular about the stator center, a rotating frame transformation can be made to make the problem quasi-steady. Figure 1 shows a cross section of an annular seal with a whirling rotor, with a spin speed $\omega_x$, a whirl speed $\Omega_x$, and an orbit radius $\varepsilon$. A coordinate frame $Y'$–$Z'$ is attached to the rotor (Fig. 2) such that the $Y'$ axis always lies along a line joining the stator center and the minimum-clearance point. The positions of the rotor and the coordinates $Y'$–$Z'$ at two time instances are also shown. Obviously, in the $Y'$–$Z'$ plane the flow domain does not change shape. Since the minimum- clearance point rotates at the whirl speed $\Omega_x$, the frame $X'$–$Y'$–$Z'$ also rotates about the $X$ axis at $\Omega_x$.

The rotor and stator wall velocities in the rotating frame are calculated as follows: Referring to Fig. 1, the absolute velocities of the rotor and stator walls can be written as

$$\vec{v}_{s,a} = 0 \tag{1}$$

$$\vec{v}_{r,a} = \vec{\omega}_x \times \vec{r}_r + \vec{\Omega}_x \times \vec{\varepsilon} \tag{2}$$

where $\vec{r}_r$ is the position vector of a rotor wall point with respect to the rotor center. To get the velocities in the rotating frame, one needs to subtract a velocity $\vec{u}_\theta$ of the form

$$\vec{u}_\theta = \vec{\Omega}_x \times \vec{R} \tag{3}$$

from all velocities, where $\vec{R}$ is the position vector with respect to the stator center. Thus, the stator and rotor wall velocities in the relative frame become

$$-\vec{v}_{s,r} = \vec{\Omega}_x \times \vec{R}_s \tag{4}$$

and

$$\vec{v}_{r,r} = \vec{\omega}_x \times \vec{r}_r + \vec{\Omega}_x \times \vec{\varepsilon} - \vec{\Omega}_x \times \vec{R}_r \tag{5}$$

Noting that

$$\vec{R}_r = \vec{r}_r + \vec{\varepsilon} \tag{6}$$

we get

$$\vec{v}_{r,r} = \left(\vec{\omega}_x - \vec{\Omega}_x\right) \times \vec{r}_r \tag{7}$$

Thus, we see that in the transformed plane the stator wall has a tangential velocity with respect to the stator center in the opposite direction to the whirl but that the rotor wall has a tangential velocity with respect to the rotor center. The apparent rotor spin is the difference between the rotor spin and whirl speeds. The tangential nature of the wall velocities corroborates our assertion that indeed in this frame the problem is quasi-steady. The momentum equations need to be modified to account for the

centrifugal and Coriolis accelerations resulting from the frame transformation. For a synchronous whirl $\omega_x = \Omega_x$ and the rotor surface velocity is zero. In effect, the whirling rotor problem has been reduced to a bearing problem but with the important difference that the rotor is stationary and the stator is spinning. This fact is crucial in understanding the flow physics and will be used in a later section to explain the observed results.

## 4. FLOW AND BOUNDARY CONDITIONS

Turbulent flow solutions were obtained for one of the flow conditions considered in the experimental data [15–16]. The experimental rig and procedures are described in [15–16]. The seal dimensions were $L$ = 37.3 mm, $R$ = 82.05 mm, and clearance $C$ = 1.27 mm. The whirl orbit radius $\varepsilon$ was one-half of $C$. Two different grids were used in the computations. The numbers of axial and tangential cells were 40 and 20, respectively. In the radial direction 16 and 30 cells were used for the standard and low-Re models, respectively. A higher number of cells in the $\theta$ direction would have been preferable, but the experimental data were available at only 20 tangential stations and hence 20 cells were used to expedite the interpolation of the experimental data at the inlet and exit boundaries.

The working fluid was water with density $\rho$ = 996 kg/m$^3$ and dynamic viscosity $\mu = 7.83\times10^{-4}$ Pa–s. The fluid was taken as incompressible and with constant properties. Convective fluxes were discretized using the central differencing method with 20% damping (upwinding). Results presented here are for a rotor spin and whirl speed of 3600 rpm, which corresponds to a Taylor number of 6600. The mean axial velocity was 7.4 m/s, which corresponds to a Reynolds number of 24 000.

Experimentally measured profiles of $u_r$, $u_\theta$, $u_x$, and $k$ were imposed at the seal inlet. A cubic spline interpolation procedure was used to curve fit the experimental data in the radial direction. The experimental data had to be modified because they were sparse and because the point nearest the wall was still quite far from the wall. Periodic boundary conditions were used in the $\theta$ direction. Static pressure was specified at the exit boundary. Experimental distribution of static pressure in the $\theta$ direction was used. Transformed wall boundary velocities were imposed on the rotor and stator walls. As described earlier the rotor wall velocities were zero, and the stator velocities corresponded to a spin at a rotational speed of $-\Omega_x$.

## 5. RESULTS AND DISCUSSION

Results presented here are the stator wall pressures and the contours of normalized axial, radial, and tangential velocities at several cross sections along the seal length. The axial $u_x$ and radial $u_r$ velocities were normalized with the mean axial velocity $U_m$, and the tangential velocity $u_\theta$ was normalized with the rotor surface tangential velocity $w_{sh}$.

Figure 3 shows the distribution of the axial velocities computed by using the standard $k$-$\varepsilon$ model. The corresponding experimental data are shown in Fig. 4. The inlet plane shows a peak velocity region on the suction side of the seal. This is physically consistent, since plenum flow will accelerate along the highest negative axial pressure gradient on the suction side. With increasing axial distance the peak axial velocity magnitude drops, and the peak region spreads in the larger clearance area ($X/L$=0.49). Further downstream the peak velocity increases again, and the peak region contracts and moves toward the pressure side of the seal. The calculated axial velocities are in good agreement with the data, in terms of both the magnitude and location of the peak velocity. The numerical results show a thicker boundary layer in the early portion of the seal; this could be due in part to the coarseness of the grids, the effect of inlet boundary, and the turbulence model. The results for the corresponding velocities with the low-Re model are shown in Fig. 5. These results are very close to the numerical predictions shown in Fig. 3.

At this point it should be emphasized again that this behavior must be explained in the *transformed coordinates*. In the absolute frame the shift of the maximum velocity region from the suction side (i.e., low-pressure zone) to the high-pressure side seems wrong. In addition, it is taking place in a direction opposite to that of the rotor spin and whirl in the absolute frame. This type of reasoning can easily

lead to an erroneous explanation of the results as outlined in [15–17]. Instead, one must look at the flow in the transformed frame, where the pressure gradients in the θ direction are a result of the *Couette flow* generated by the *moving stator wall*, which "drags" the maximum velocity fluid pocket in a direction opposite to the rotor spin and whirl (Fig. 3).

The normalized radial velocities for the standard $k$-ε model are shown in Fig. 6 and the experimental data in Fig. 7. The inlet plane shows some effects of the vena contracta. The radial velocities later drop to a few percent of the mean axial velocity. The double-lobed structure in the latter part of the seal may be due in part to conversion from relative to absolute velocities. The results obtained with the low-Re model (Fig. 8) are similar to the standard $k$-ε model results.

The contours of the absolute tangential velocity are shown in Fig. 9. The inlet plane shows smaller incoming swirl that gradually increases with axial distance (spreading contours) as the rotor spins the fluid up. The results show good correlation with the experimental plots in Fig. 10. The low-Re results (Fig. 11) are similar to the results in Fig. 9. The only difference is in the contours at the seal exit, where the low-Re model predicts somewhat higher tangential velocities.

The pressures on the stator wall were reported by Winslow [18], and pressure profiles from this data set were used as the exit boundary condition in the computations. The pressure on the outer wall as a function of the "time fraction" and the axial distance were measured and plots are shown in Fig. 12. The time fraction represents the circumferential location of a point on the stator wall when working with the transformed coordinates. The time fraction 0.5 corresponds to the minimum clearance; the pressure side (ahead of the rotor) is between 0 and 0.5 and the suction side is between 0.5 and 1.0. A high- pressure zone exists in the entrance region ahead of the rotor (pressure side), and a low-pressure zone exists behind the rotor. Along the seal length these zones reduce in intensity and get more evenly distributed. Near the exit of the seal the measured pressures reverse locations (i.e. the high-pressure zone comes over to the suction side of the rotor and the lower pressure is on the pressure side). In the numerical simulations the relative locations of the maximum and minimum pressures are maintained, although the difference between the two decreases. The experimental data show several "bands" along the axial directions. This feature is absent in the simulations and may be due to imperfections in the rotor surface. The absolute values of the maximum and minimum pressures are somewhat underpredicted in the simulations. Calculations show stator pressure values of $-14.2 < P^*_{calc} < 14.6$ for the standard $k$-ε model and $-12.7 < P^*_{calc} < 16.8$ for the low-Re model, both of which are in fair agreement with the experimental values, $-24.6 < P^*_{expt} < 19.4$.

## 6. SUMMARY OF RESULTS

The turbulent flow fields in a synchronously whirling annular seal were simulated by using a three-dimensional computational fluid dynamics code. A transformation to a rotating frame was done to render the flow quasi-steady. In this frame the computed flow fields showed a fair to good agreement with the experimental data and a consistent picture of the flow field and physics. Although the turbulence models used in this study assume isotropic turbulence, the models did a good job of predicting flow behavior, which clearly has anisotropic turbulence, both in qualitative and quantitative terms. Additional flow cases with other reported flow conditions and with nonisotropic turbulence models are clearly needed.

## 7. ACKNOWLEDGMENTS

These computations were performed under NASA Lewis contract NAS3–25644, entitled Study of Fluid Dynamic Forces in Seals, with R.C. Hendricks as the technical monitor. This support is greatly appreciated.

## 8. REFERENCES


1. Black, H.F., Effects of Hydraulic Forces in Annular Seals on the Vibrations of Pump Rotors, *J. Mech. Eng. Science*, Vol. 184 (1970).
2. Childs, D.W., Finite Length Solutions for Rotordynamic Coefficients of Turbulent Annular Seals, *Trans. ASME, J. Lub. Tech*, Vol. 105 (1983) 437.
3. San Andres, L.A., Analysis of Variable Fluid Properties, Turbulent Annular Seals, *Trans. ASME, J. Tribology* , Vol. 113 (1991) 694–702.
4. Tam, L.T., Przekwas, A.J., Muszynska, A., Hendricks, R.C., Braun, M.J., and Mullen, R.L., Numerical and Analytical Study of Fluid Dynamic Forces in Seals and Bearings, *Trans. ASME, J. Vibration, Acoustics, Stress and Reliability in Design* , Vol. 110 (1988) 315–325.
5. Dietzen, F.J. and Nordmann, R., Calculating Rotordynamic Coefficients of Seals by Finite Difference Techniques, *Trans. ASME, J. Tribology*, Vol. 109 (1987) 388–394.
6. Baskharone, E.A. and Hensel, S.J., A Finite-Element Perturbation Approach to Fluid/Rotor Interaction in Turbomachinery Elements, Part 1: Theory, *Trans. ASME, J. Fluids Eng.*, Vol. 113 (1991) 353–361.
7. Baskharone, E.A. and Hensel, S.J., A Finite-Element Perturbation Approach to Fluid/Rotor Interaction in Turbomachinery Elements, Part 2: Applications, *Trans. ASME, J. Fluids Eng.*, Vol. 113 (1991) 365–367.
8. Athavale, M.M., Przekwas, A.J., and Singhal, A.K., Development of a CFD Code for Analysis of Fluid Dynamic Forces in Seals, *Proc. Workshop on Seals Flow Code Development*, NASA CP–10070 (1991).
9. Athavale, M.M., Przekwas, A.J., Hendricks, R.C., and Liang, A., SCISEAL: A Three-Dimensional CFD Code for Accurate Analyses of Fluid Flow and Forces in Seals, *Proc. Advanced Earth-to-Orbit Propulsion Conference*, NASA CP–3282 (1994) 337–345.
10. Athavale, M.M. and Hendricks, R.C., A Small Perturbation CFD Method for Calculation of Seal Rotordynamic Coefficients, *Proc. 5th Int. Symp. on Transport Phenomena and Dynamics of Rotating Machinery* (1994).
11. Falco, M., Mimmi, G., and Mareno, G., Effects of Seals on Rotordynamics, *Proc. Int. Conf. on Rotordynamics* (1986).
12. Kanemori, Y. and Iwatsubo, T., Experimental Study of Dynamic Fluid Forces and Moments for a Long Annular Seal, *Trans. ASME, J. Tribology*, Vol. 114 (1992) 773–778.
13. Morrison, G.L., Johnson, M.C., and Tatterson, G.B., Three-Dimensional Laser Anemometer Measurements in an Annular Seal, *Trans. ASME, J. Tribology*, Vol. 113 (1991) 421–427.
14. Morrison, G.L., Johnson, M.C., and Tatterson, G.B., 3–D Laser Anemometer Measurements in a Labyrinth Seal, *Trans. ASME, J. Eng. for Gas Turbines and Power*, Vol. 113 (1991) 119–125.
15. Thames, H.D., III, Mean FLow and Turbulence Characteristics in Whirling Annular Seals, M.S. Thesis, Texas A&M University (1992).
16. Morrison, G.L., DeOtte, R.E, Jr., and Thames, H.D., III, Experimental Study of the Flow Field Inside a Whirling Annular Seal, *Tribology Trans.*, Vol. 37 (1994) 425–429.
17. Morrison, G.L. and Shreshta, S., Measure of Turbulence in Shaft Seals, *Proc. Advanced Earth-to-Orbit Propulsion Conference*, NASA CP–3282 (1994) 356–362.
18. Winslow, R.B., Dynamic Pressure and Shear Stress Measurements on the Stator Wall of Whirling Annular Seals, M.S. Thesis, Texas A&M University (1994).

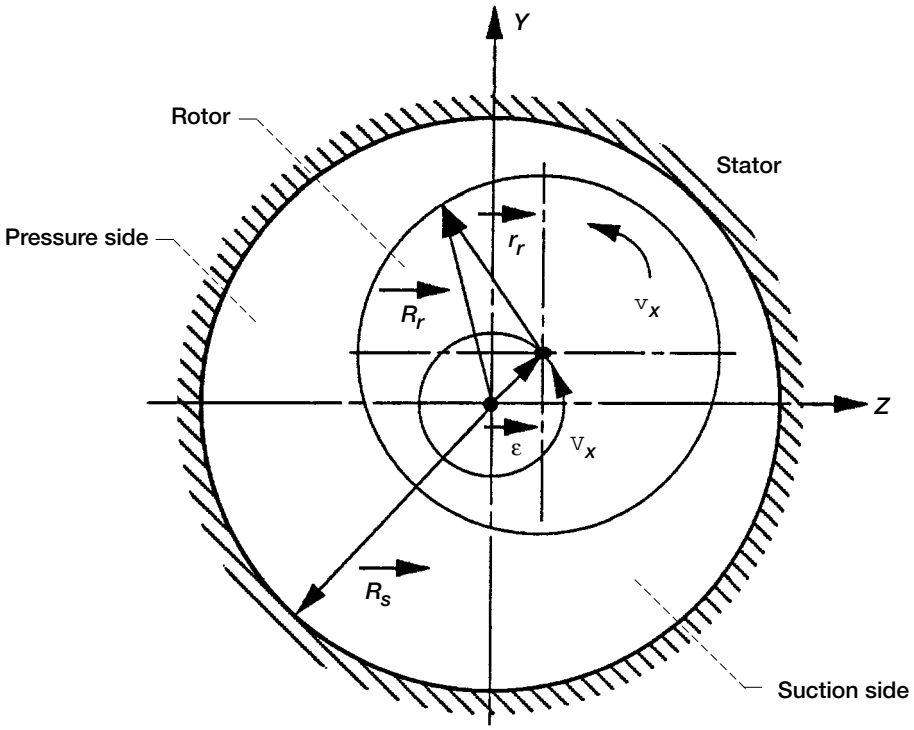


Figure 1.—Details of annular seal with whirling rotor. Axial flow and *x* axis point into plane of paper.

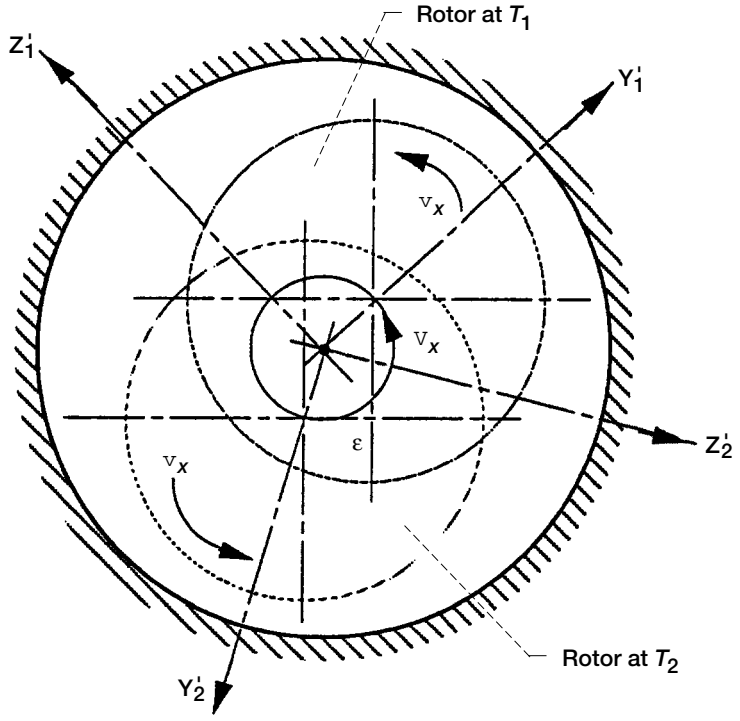


Figure 2.—Rotor positions and associated coordinate frames at two different times, $T_1$, $T_2$.

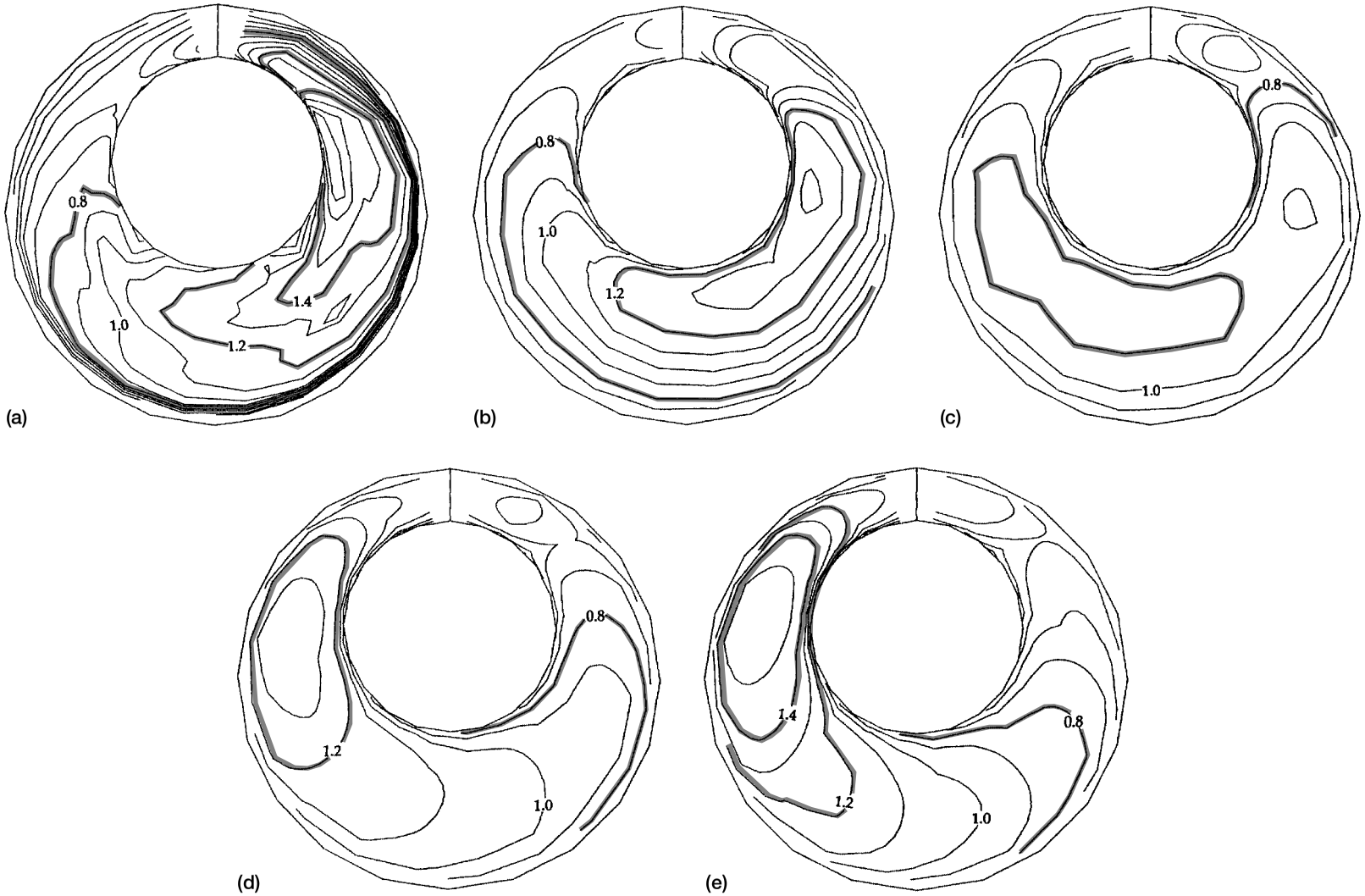


Figure 3.—Normalized axial velocity contours $u_x^*$ at different seal sections using standard $k$-$\varepsilon$ model. (a) $X/L$ = 0.00125. (b) $X/L$ = 0.2125. (c) $X/L$ = 0.4875. (d) $X/L$ = 0.7625. (e) $X/L$ = 0.9825.

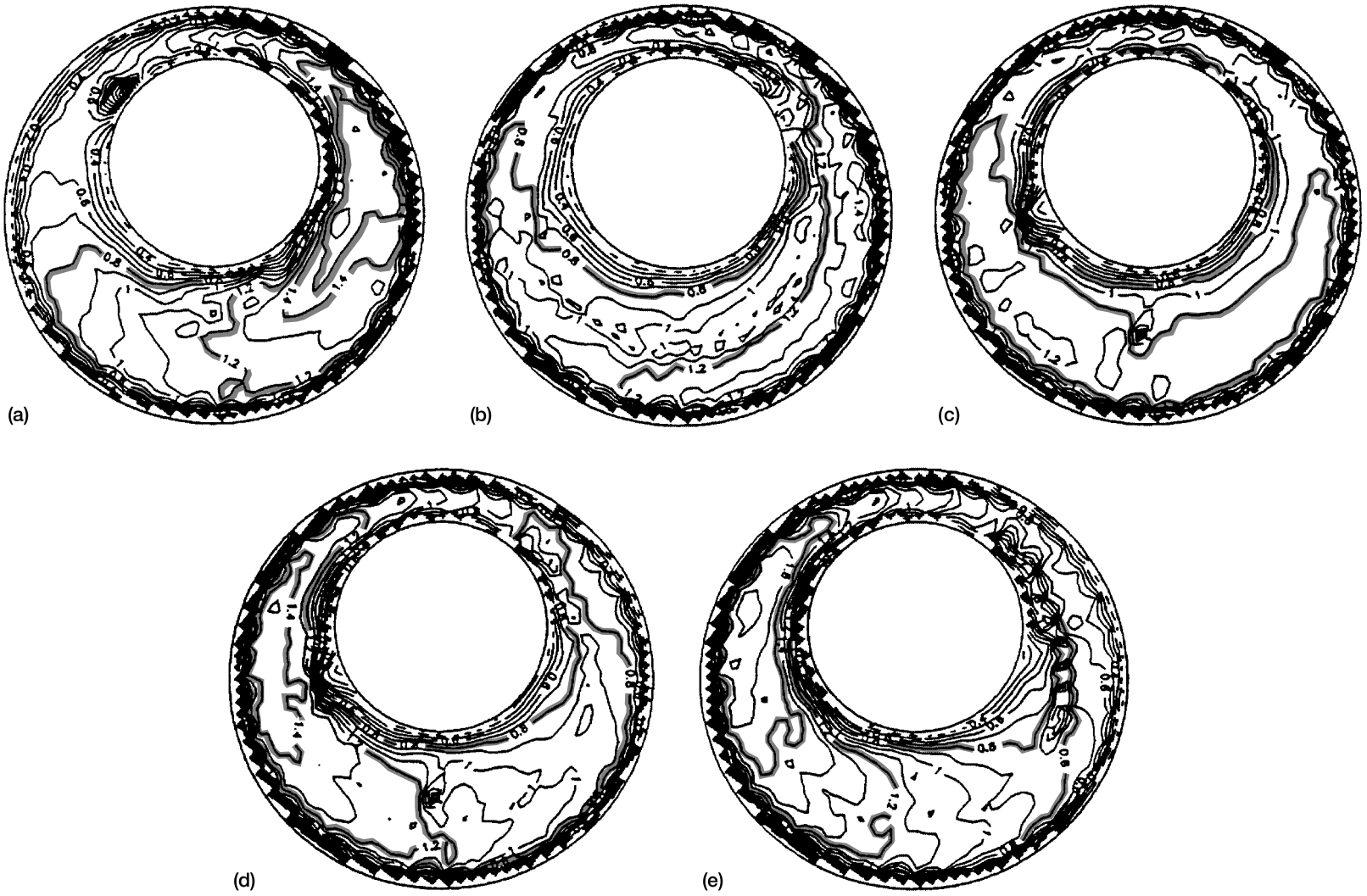


Figure 4.—Experimental data for normalized axial velocity [15, 16]. (a) $X/L$ = 0. (b) $X/L$ = 0.22. (c) $X/L$ = 0.49. (d) $X/L$ = 0.77. (e) $X/L$ = 0.99.

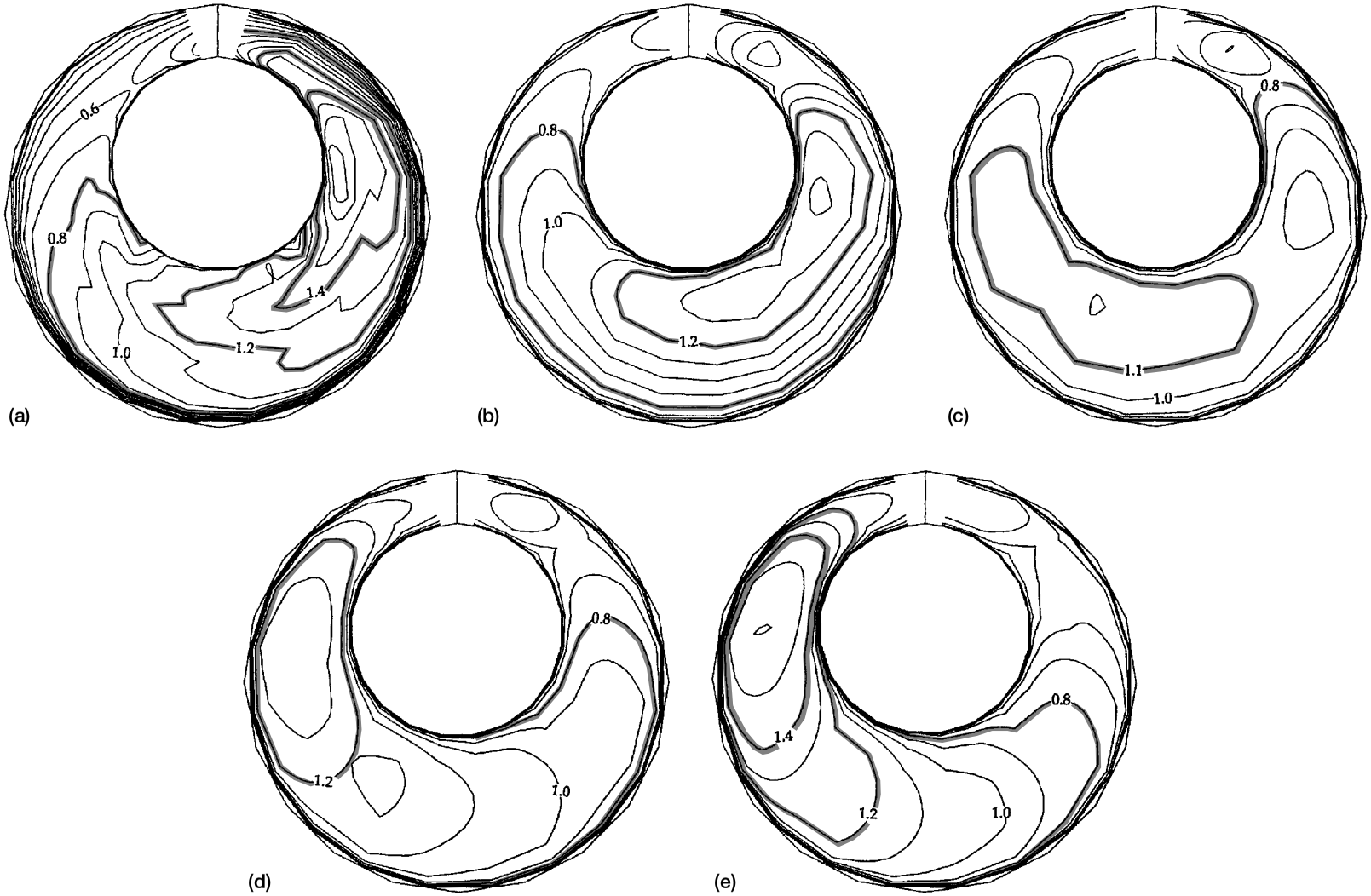


Figure 5.—Normalized axial velocity contours using low-Re model. (a) *X/L* = 0.00125. (b) *X/L* = 0.2125. (c) *X/L* = 0.4875. (d) *X/L* = 0.7625. (e) *X/L* = 0.9875.

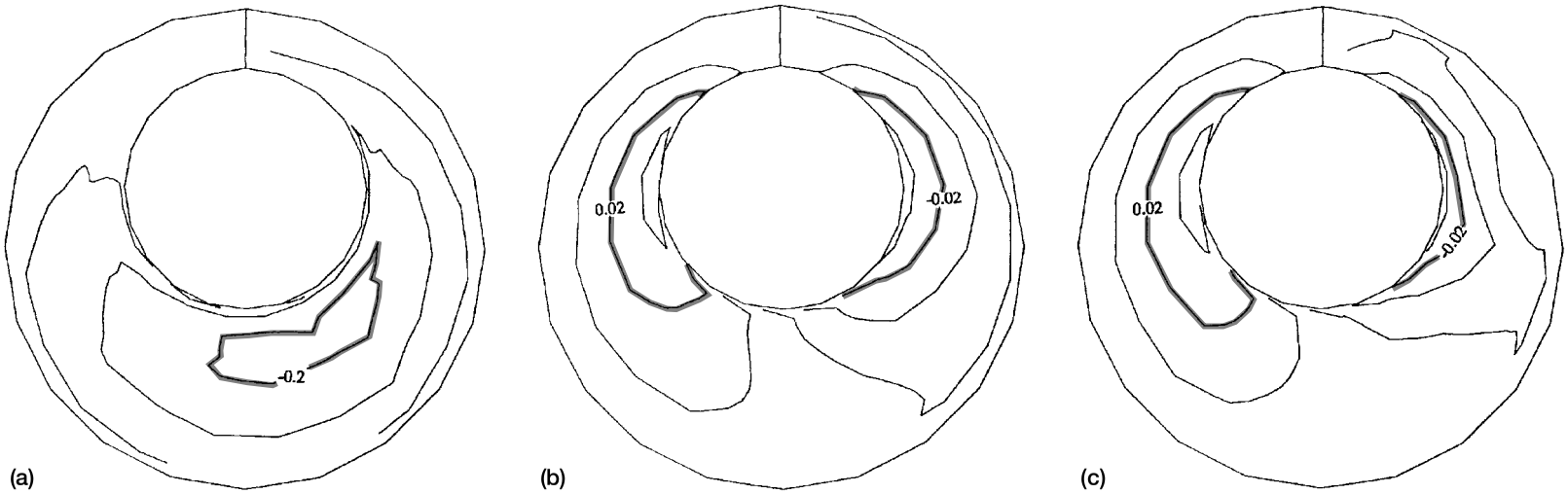


Figure 6.—Normalized radial velocity $u'_r$ contours using standard $k$-$\varepsilon$ model. (a) $X/L$ = 0.00125. (b) $X/L$ = 0.4875. (c) $X/L$ = 0.9875.



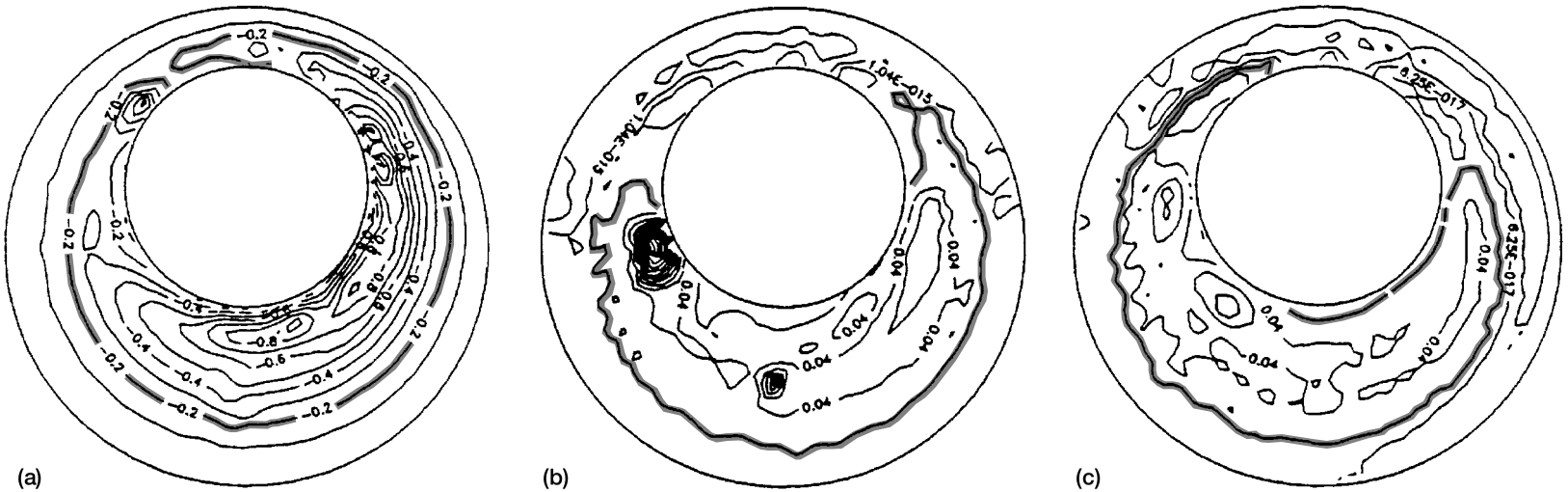


Figure 7.—Normalized radial velocity $u'_r$ contours using experimental data [15, 16]. (a) $X/L$ = 0. (b) $X/L$ = 0.49. (c) $X/L$ = 0.99.

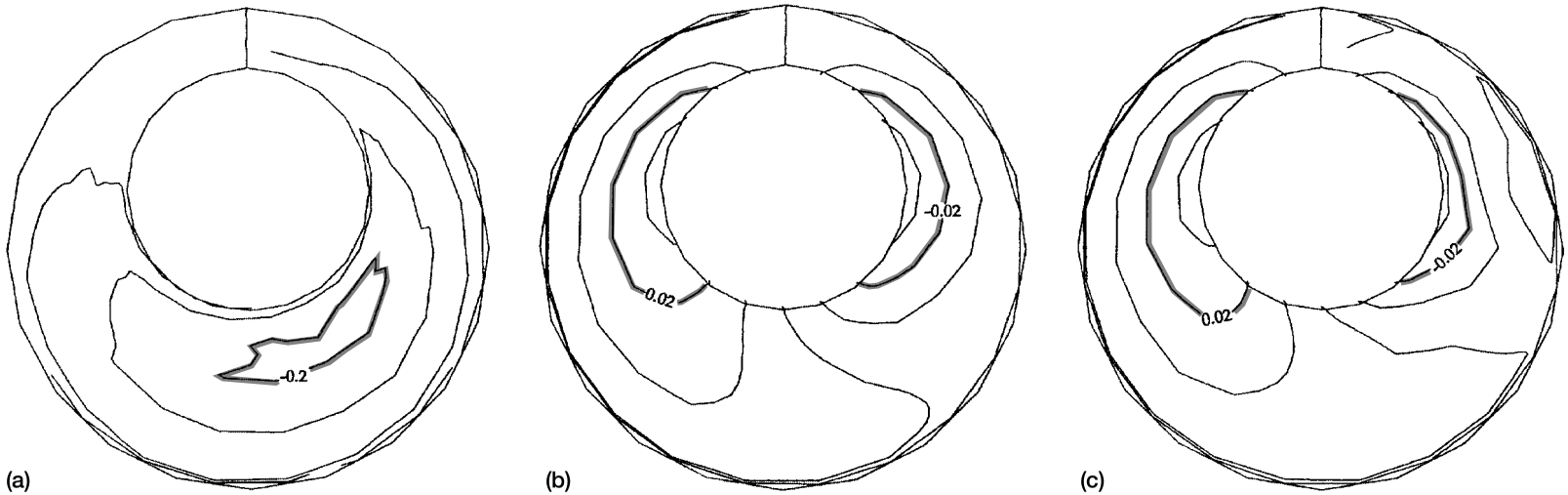


Figure 8.—Normalized radial velocity $u_r^*$ contours using low-Re model. (a) *X*/*L* = 0.00125. (b) *X*/*L* = 0.4875. (c) *X*/*L* = 0.9875.



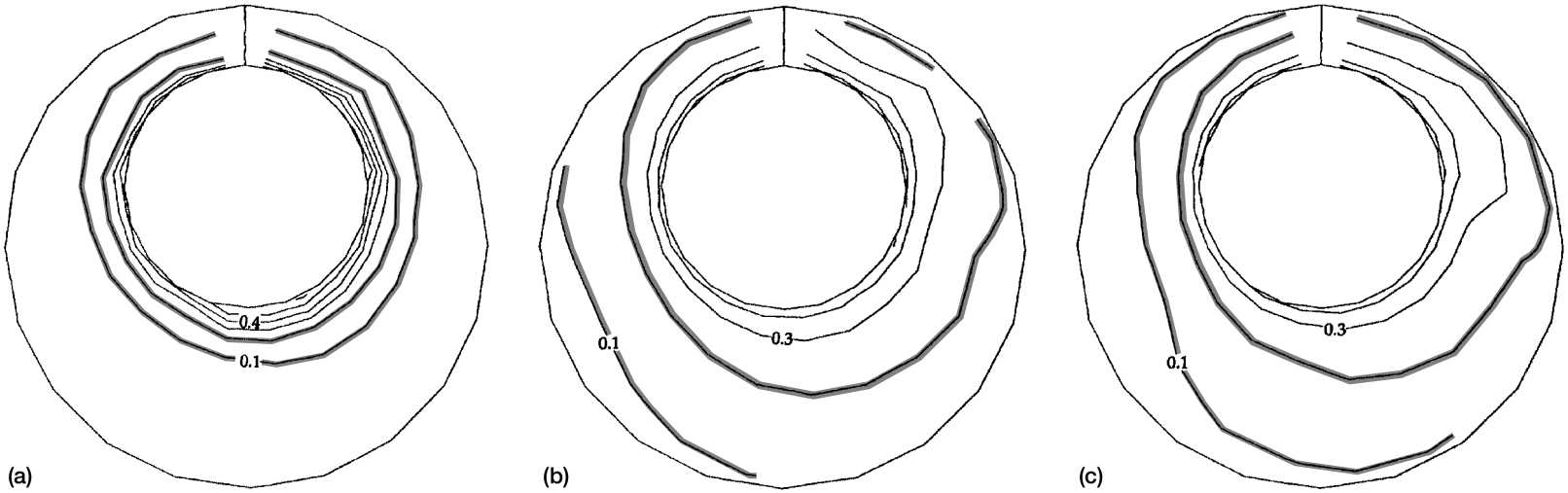


Figure 9.—Normalized tangential velocity $u_u^*$ contours using standard *k*-ε model. (a) *X*/*L* = 0.00125. (b) *X*/*L* = 0.4875. (c) *X*/*L* = 0.9875.

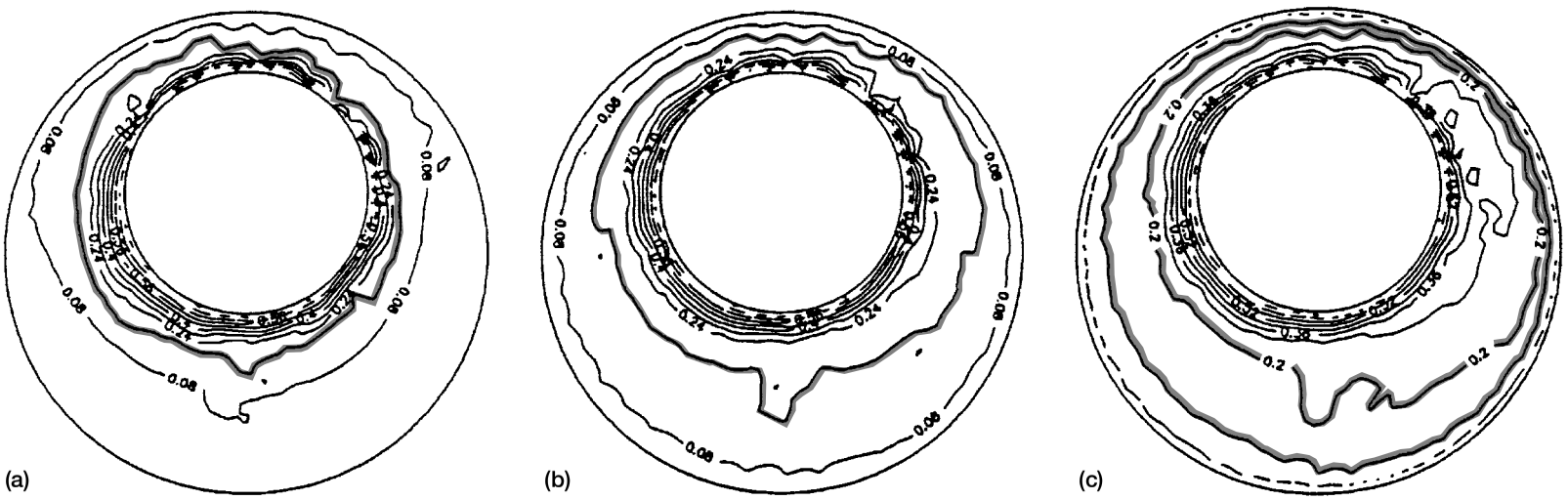


Figure 10.—Normalized tangential velocity $u_{\tilde{u}}^{\star}$ contours using experimental data [15, 16]. (a) $X/L$ = 0. (b) $X/L$ = 0.49. (c) $X/L$ = 0.99.

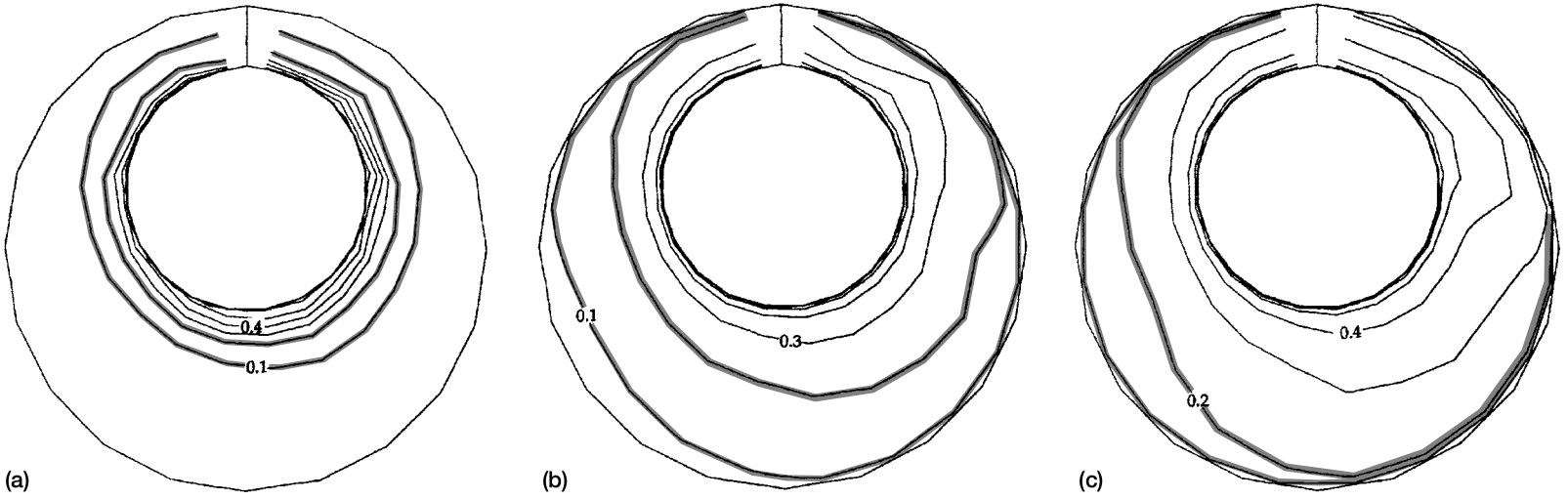


Figure 11.—Normalized tangential velocity $u_{\tilde{u}}^{\star}$ contours using low-Remodel. (a) $X/L$ = 0.00125. (b) $X/L$ = 0.4875. (c) $X/L$ = 0.9875.

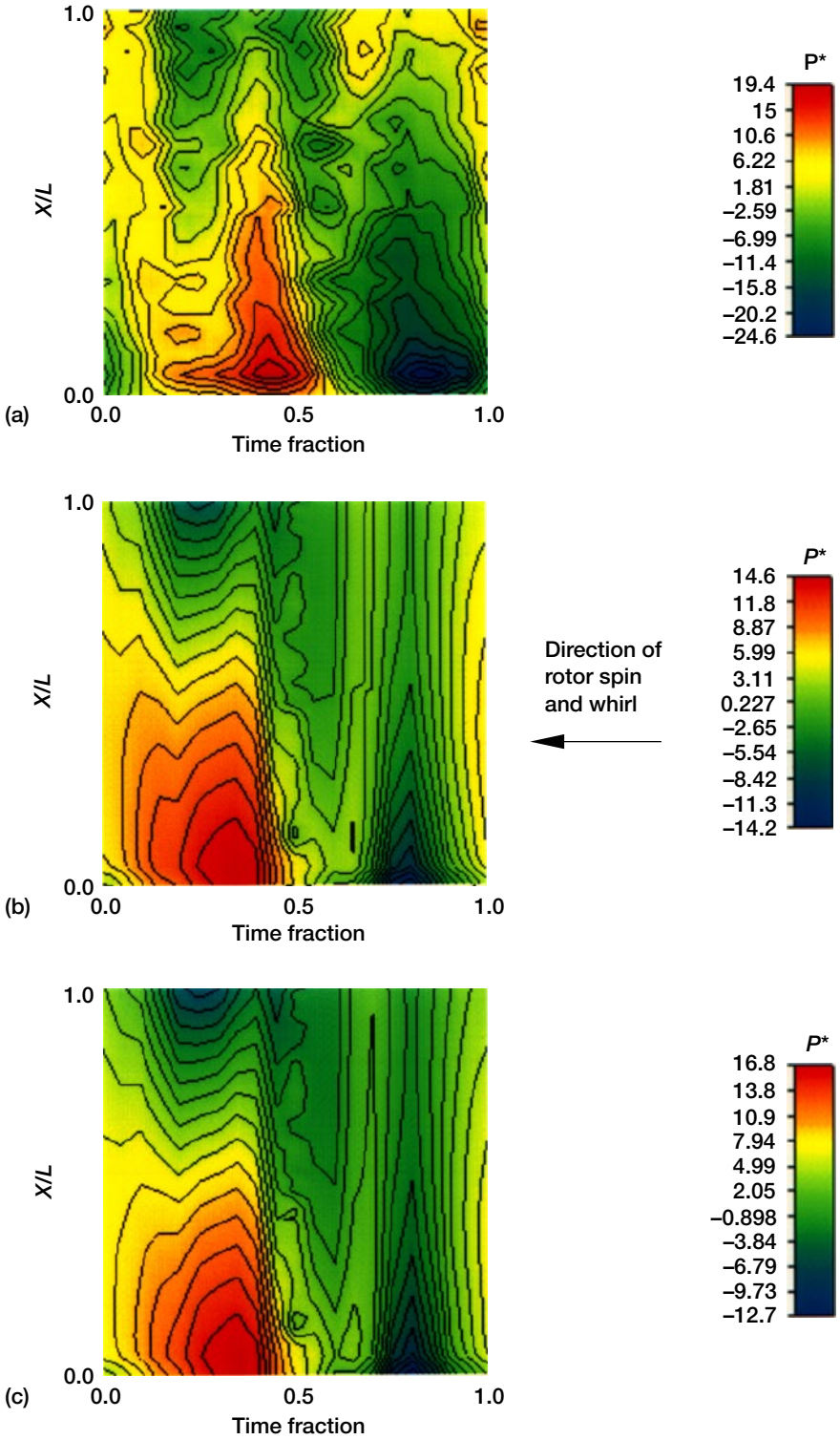


Figure 12.—Stator wall pressures as a function of axial and tangential distance. Time fraction 0.5 is at minimum clearance, 0 to 0.5 is pressure side, and 0.5 to 1.0 is suction side. (a) Experimental data. (b) Standard $k$-$\varepsilon$ model results. (c) Low-Re model results.

# REPORT DOCUMENTATION PAGE

*Form Approved*
*OMB No. 0704-0188*



| 1. AGENCY USE ONLY (*Leave blank*) | 2. REPORT DATE | 3. REPORT TYPE AND DATES COVERED |
|---|---|---|
| | March 1996 | Technical Memorandum |

**4. TITLE AND SUBTITLE**

Numerical Simulation of Flow in a Whirling Annular Seal and Comparison With Experiments

**5. FUNDING NUMBERS**

WU–242–20–06

**6. AUTHOR(S)**

M.M. Athavale, R.C. Hendricks, and B.M. Steinetz

**7. PERFORMING ORGANIZATION NAME(S) AND ADDRESS(ES)**

National Aeronautics and Space Administration
Lewis Research Center
Cleveland, Ohio 44135–3191

**8. PERFORMING ORGANIZATION REPORT NUMBER**

E–10026

**9. SPONSORING/MONITORING AGENCY NAME(S) AND ADDRESS(ES)**

National Aeronautics and Space Administration
Washington, D.C. 20546–0001

**10. SPONSORING/MONITORING AGENCY REPORT NUMBER**

NASA TM–107117

**11. SUPPLEMENTARY NOTES**

Prepared for the Sixth International Symposium on Transport Phenomena and Dynamics of Rotating Machinery cosponsored by the Pacific Center of Thermal Fluids Engineering and the U.S. Turbo and Power Machinery Research Center, Honolulu, Hawaii, February 25–29, 1996. M.M. Athavale, CFD Research Corporation, Huntsville, Alabama 35805 (work funded by NASA Contract NAS3–25644); R.C. Hendricks and B.M. Steinetz, NASA Lewis Research Center. Responsible person, R.C. Hendricks, organization code 5300, (216) 977–7507.

**12a. DISTRIBUTION/AVAILABILITY STATEMENT**

Unclassified - Unlimited
Subject Categories 07 and 20

This publication is available from the NASA Center for Aerospace Information, (301) 621–0390.

**12b. DISTRIBUTION CODE**

**13. ABSTRACT** ***(Maximum 200 words)***

The turbulent flow field inside a whirling annular seal was simulated by using SCISEAL, a three-dimensional computational fluid dynamics code. The rotor center described a circular synchronous whirl. A rotating frame transformation was used to make the problem quasi-steady. The flow field at an axial Reynolds number of 24 000 and a Taylor number of 6600 was simulated. The standard $k$–$\varepsilon$ model with wall functions and the low-Reynolds-number model were used to treat turbulence. An experimentally measured velocity field was used at the inlet boundary. Numerical predictions of the velocities and the stator wall pressures compared well with experimental data. Both turbulence models yielded nearly the same results. The capability of the SCISEAL code to analyze this complex flow field was demonstrated; the isotropic turbulence models performed adequately on this nonisotropic turbulence flow.

| 14. SUBJECT TERMS | 15. NUMBER OF PAGES |
|---|---|
| Seal; Rotordynamics; CFD; Turbulence; Modeling; Bearings; Tribology | 16 |
| | 16. PRICE CODE: A03 |

| 17. SECURITY CLASSIFICATION OF REPORT | 18. SECURITY CLASSIFICATION OF THIS PAGE | 19. SECURITY CLASSIFICATION OF ABSTRACT | 20. LIMITATION OF ABSTRACT |
|---|---|---|---|
| Unclassified | Unclassified | Unclassified | |